Ⓔ

Coulomb Stress Change and Evolution Induced by the 2008 Wenchuan Earthquake and its Delayed Triggering of the 2013 M_w 6.6 Lushan Earthquake

by Yanzhao Wang, Fan Wang, Min Wang, Zheng-Kang Shen, and Yongge Wan

Online Material: Table of GPS velocities.

INTRODUCTION

Almost five years after the 12 May 2008 M_w 7.9 Wenchuan earthquake, the Longmenshan fault zone was struck by the April 20 M_w 6.6 Lushan earthquake, with its hypocenter located ~45 km southwest of the southern end of the Wenchuan surface rupture (Han *et al.*, 2014; Zhang *et al.*, 2014; Fig. 1). Such proximity in space and time between the two events implies that the later event is an aftershock of the previous one, or in other words, the previous event played a more important role in the occurrence of the latter than the long-term tectonic loading did. Early studies on the problem had split opinions. On one hand, Du *et al.* (2013), Liu *et al.* (2013), and Xu *et al.* (2013) considered the two earthquakes as independent events. Wang *et al.* (2013) and Parsons and Segou (2014), on the other hand, claimed that the Lushan earthquake should be viewed as an aftershock of the Wenchuan earthquake. Whereas each group has its own basis of reasoning, lack of quantitative examination makes these claims less convincing. In recent years, Coulomb stress change has been widely used in estimating magnitude of stress loading for identification of areas or structures at increased risk of earthquake triggering (e.g., Harris, 1998; Stein, 1999; Chéry *et al.*, 2001; Freed and Lin, 2001; Pollitz and Sacks, 2002; Freed, 2005; Steacy *et al.*, 2005; Gomberg and Felzer, 2008). In this paper, we apply this method to investigate to what extent the Lushan earthquake has been triggered by the Wenchuan earthquake. Previous studies have explored the consequence of the 2008 Wenchuan earthquake on the changes in Coulomb stresses on the major faults in the region (Parsons *et al.*, 2008; Toda *et al.*, 2008; Luo and Liu, 2010; Wan and Shen, 2010; Xu *et al.*, 2010; Nalbant and McClosky, 2011). These studies indicated that both coseismic rupture and postseismic viscoelastic relaxation of the 2008 Wenchuan earthquake may have significantly increased/decreased stress levels on some neighborhood faults. Here we calculate both the coseismic and postseismic Coulomb stress changes caused by the 2008 Wenchuan earthquake based on a 3D viscoelastic model with updated coseismic slip distribution, and compare these contributions with the tectonic stress loading accumulated since the Wenchuan earthquake to assess the significance of the triggering effect of the Wenchuan earthquake.

EVALUATING COULOMB STRESS CHANGE

In this paper, we calculate the Coulomb stress change and evolution in the western Sichuan, China region induced by the 2008 Wenchuan earthquake. The active-fault model is adopted from Deng *et al.* (2007), with some simplification. Particularly for the surface locations of the Longmenshan fault zone in our model, we employ the surface rupture trace of the 2008 Wenchuan earthquake along the main fault (Shen *et al.*, 2009) and the surface trace of rupture zone of the 2013 Lushan earthquake resolved by Z. Jiang *et al.* (unpublished report, 2013; see Data and Resources). Vertical faults are assumed for strike-slip dominant faults, which include most of the faults in the region; and slant faults are prescribed for the Longmenshan and Daliangshan faults, whose dip angles are 38°–90° and 75°, respectively. We use the PSGRN/PSCMP code provided by Wang *et al.* (2006) and an updated coseismic slip model of the Wenchuan earthquake (Shen, Wang, *et al.*, 2011) using data provided by Shen *et al.* (2009) and Wang *et al.* (2011) to calculate stress evolution after the Wenchuan earthquake. The viscoelastic structure of the lithosphere in the model is illustrated in Figure 2. We did not consider afterslip effect in this calculation, because its contribution is not very large compared with that of the mainshock (Shen *et al.*, 2009) and is concentrated in near field due to its relatively shallow origin in comparison with the viscous relaxation (Shen, Wang, *et al.*, 2011). Most of the aftershock contributions have been accounted for implicitly, because the coseismic slip model was constrained by

 doi: 10.1785/0220130111

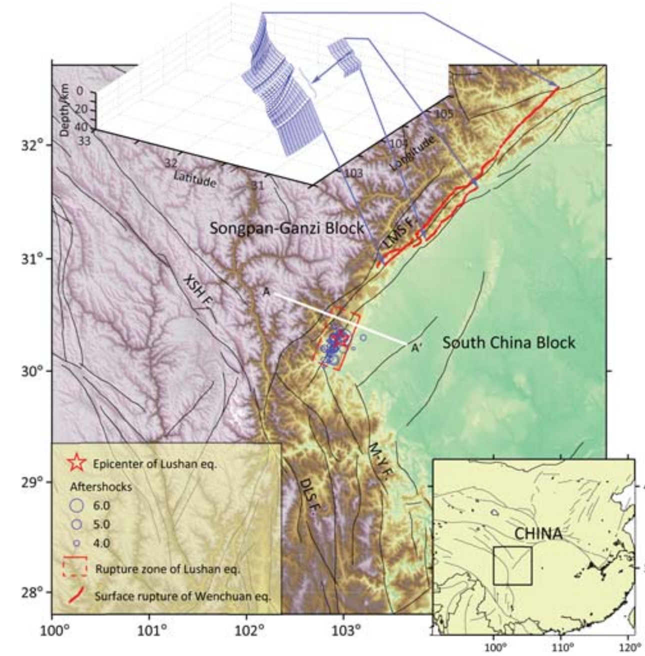

▲ **Figure 1.** Topography and fault map of the study area. Black curves are quaternary faults. Red curves mark the surface rupture trace of the Wenchuan earthquake with an inset sketch showing the earthquake source model (Shen, Wang, *et al.*, 2011). A red rectangle denotes the rupture zone of the Lushan earthquake (Jiang *et al.*, submitted). The thick white line A–A′ shows the position of the cross section in Figure 2. Abbreviations are: LMS F, the Longmenshan fault; XSH F, the Xianshuihe fault; DLS F, the Daliangshan fault; and M–Y F, the Mabian–Yanjin fault.

data collected a few weeks or even months after the mainshock, by then most of the large aftershocks occurred already. Those occurred in later times after the geodetic data collection (whose magnitudes are 6 or less) would result in regional stress changes which are much smaller than that predicted by the coseismic model adopted here.

From the Coulomb friction criterion, the Coulomb failure stress change (ΔCFS) on a fault interface is defined as

$$\Delta \mathrm{CFS} = \Delta\tau_s + \mu(\Delta\sigma_n + \Delta p), \tag{1}$$

in which $\Delta\tau_s$ is the change of shear stress, $\Delta\sigma_n$ the change of normal stress (positive for extension), μ the friction coefficient, and Δp the change of pore pressure (Stein *et al.*, 1992; King *et al.*, 1994). The effect of friction reduction due to pore pressure can be represented by an equivalent friction coefficient $\mu' = \mu(1 - B)$, in which B is the Skempton coefficient, in the range of 0–1 (Rice, 1992). Equation (1) therefore becomes

$$\Delta \mathrm{CFS} = \Delta\tau_s + \mu'\Delta\sigma_n. \tag{2}$$

In our calculation, we project the earthquake induced stress change first onto a fault plane, then to the slip direction of that fault. The $\Delta\tau_s$ is positive if it is in alignment with the fault-slip direction and vice versa. The slip directions of the fault segments are adopted from Deng *et al.* (2007). We assume $\mu' = 0.0$, 0.4, and 0.8 and evaluate the ΔCFS on faults, and assess how variation of this parameter would affect the results. We finally assess seismic potential changes on faults by comparison between Coulomb stress variations induced by the earthquake and the long-term tectonic loading, in terms of advancing/delay times of earthquake recurrence.

ESTIMATING ADVANCE/DELAY TIMES OF EARTHQUAKE RECURRENCE

Under a linear Coulomb stress loading assumption, we can use present day tectonic deformation rates to convert the earthquake-induced ΔCFS on faults into the advance/delay times to the next characteristic earthquake on the fault segments. Such assessments are done in three steps for a selection of faults.

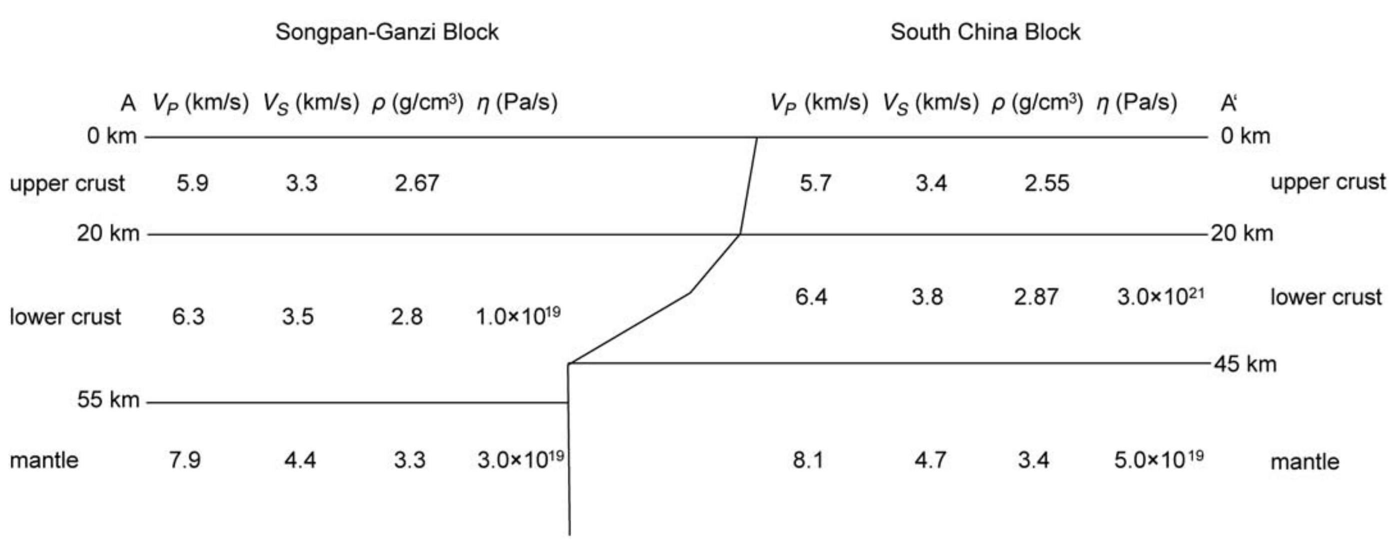

▲ **Figure 2.** Schematic illustration of lithosphere structure in the model after Shen, Wang, *et al.* (2011).

First, we collect all the Global Positioning System (GPS) data available in the region and process the data to obtain an updated interseismic horizontal-velocity field for the estimation of secular slip rates across faults. Combined with GPS data from the International Global Navigation Satellite Systems Service tracking stations, GPS data in the region are processed to obtain station positions and velocities with respect to a global reference frame (Shen, King, *et al.*, 2011). Stations located in the vicinities of strong earthquakes, such as the Wenchuan earthquake, also have their coseismic offsets and postseismic displacements (modeled as logarithmic decays) estimated. Regional station velocities are subsequently transformed to the South China reference frame using angular rotation rate of the South China block calculated from the velocities of GPS sites located within the block. Ⓔ This GPS horizontal-velocity dataset is provided in the supplementary material (Table S1 in supplement).

To estimate interseismic fault slip rates we select eight GPS velocity profiles across the Longmenshan, Xianshuihe, Daliangshan, and Mabian–Yanjin faults (Fig. 3). For better visualization the station velocities are rotated to reference to the South China block for the profiles across the Longmenshan, Daliangshan, and Mabian–Yanjin faults, and to the Songpan–Ganzi block for the profile across the Xianshuihe fault. Such rotations are done by selecting stations located in the reference block, computing the Euler rotation vector using these station velocities, and removing the rigid block rotation predicted using the Euler rotation vector from the station velocities. GPS station velocities within eight rectangles spanning the fault segments are decomposed into strike-parallel and strike-normal components, respectively, as shown in Figure 3. Surface velocity field associated with an infinitely long fault locked above a depth H and creeping underneath at a rate S in a half-space is in the form of $D(x) = 2S/\pi \, \mathrm{atan}(x/H)$ (Savage and Burford, 1973), in which x is the distance from the fault in fault-normal direction and H is determined as 20 km. According to this formula, decomposed GPS velocities are inverted for secular slip rates across the northeastern (0.3 ± 0.4 dextral and 1.2 ± 0.3 mm/yr shortening), central (0.3 ± 0.4 dextral and 2.9 ± 0.5 mm/yr shortening), and southwestern (0.4 ± 0.5 sinistral and 3.0 ± 0.4 mm/yr shortening) segments of the Longmenshan fault. The inversion was done for the northwestern (10.7 ± 1.0 sinistral and 2.6 ± 1.6 mm/yr extensional), central (10.4 ± 1.1 sinistral and 0.0 ± 0.7 mm/yr),

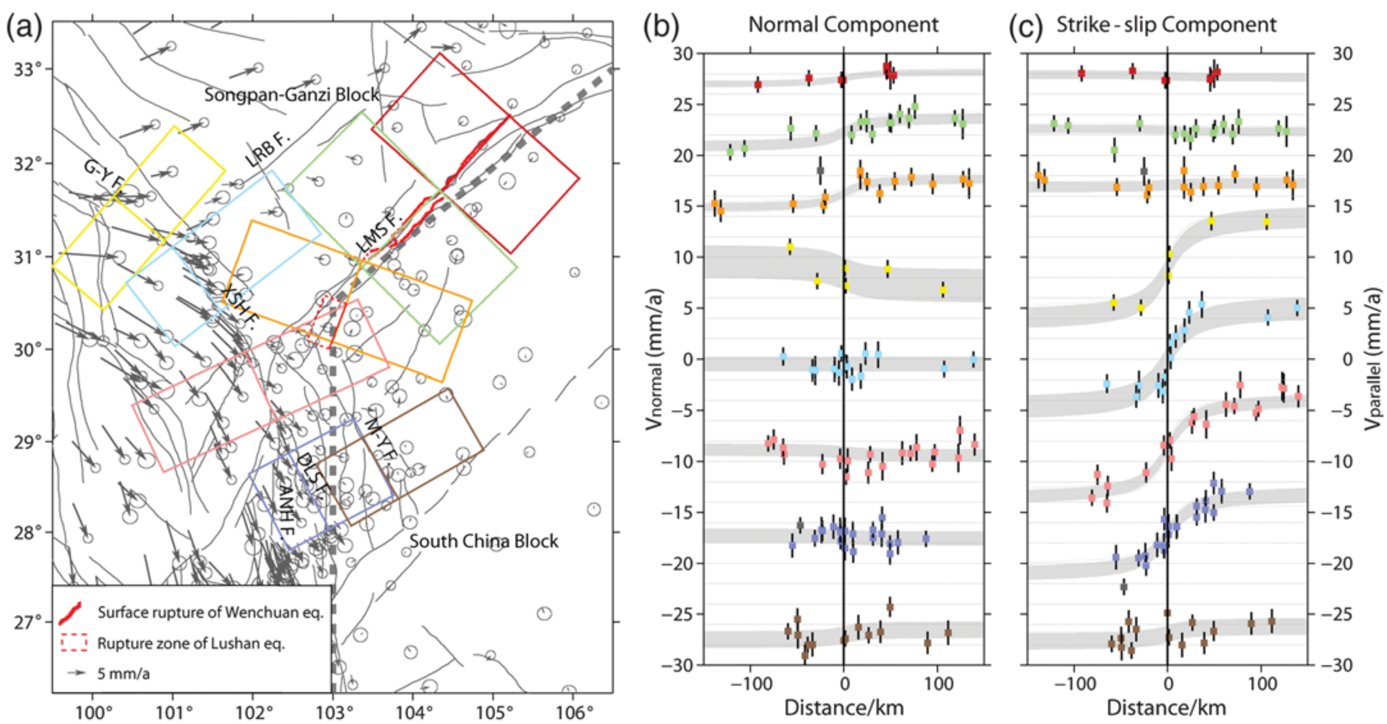

▲ **Figure 3.** GPS horizontal-velocity field and velocity profiles across faults. (a) Arrows are GPS velocities with respect to the South China block, for which the Euler vector is calculated using velocities of GPS sites within the region southeast of the dashed line boundary. Error ellipses at the ends of the arrows represent 70% confidence. Rectangular frames encompassing fault segments mark the regions within which stations are depicted for slip-rate estimation and their velocity profiles are shown in (b) fault normal, extensional positive; and (c) fault parallel, sinistral positive. Squares with the same color as that of the corresponding frame represent data used for calculating fault-slip rates, and gray squares are those eliminated from the calculation due to contamination by activities of other faults. Gray curves show the predicted displacements across fault segments calculated using estimated fault-slip rates and fault-locking depth. Widths of the curves are proportional to the displacement uncertainties. Abbreviations are: LRB F, the Longriba fault; G–Y F, the Ganzi–Yushu fault; and ANH F, the Anninghe fault.

and southeastern (10.2 ± 0.6 sinistral and 0.6 ± 0.6 mm/yr extensional) segments of the Xianshuihe, Daliangshan (8.3 ± 0.7 sinistral and 0.3 ± 0.7 mm/yr extensional), and Mabian–Yanjin (1.6 ± 0.8 sinistral and 1.1 ± 0.8 mm/yr shortening) faults, respectively (Fig. 3).

Second, we convert the secular fault-slip rates into strain accumulation rates on faults at depth. This is done assuming steady slips across faults in an elastic half-space, and the formulae and computing code of Okada (1992) are adopted to calculate the strain-rate field induced by long-term tectonic loading. In each calculation, the fault is assumed to have the same dip angles as that used in CFS calculation, slipping on a plane of 20–2000 km in depth range and 1500 km in lateral length. The fault plane extension in width and length is necessary to eliminate the edge effect and account for the full contribution across the fault system.

Third, we convert the strain-rate field to Coulomb stress rate $\dot{\tau}'$ (in the form of Equation 2 with stress components replaced by stressing rate components, as shown in Figs. 4c, 5c, and 6c) on faults with media property prescribed as 3×10^{10} Pa for shear modulus and 0.25 for Poisson's ratio, and estimate the advance/delay times of earthquake recurrence on faults using a formula $\Delta T = \Delta\mathrm{CFS}/\dot{\tau}'$ (Figs. 4d, 5d, and 6d).

Because the values of ΔCFSs span in a wide range of -10^6–10^6 Pa, we construct a function of ΔCFS and plot it using logarithmic scale for better visualization in Figures 4–6a,b, and 7:

$$f(\Delta\mathrm{CFS}) = \begin{cases} -\log(|\Delta\mathrm{CFS}| + 1), & \Delta\mathrm{CFS} < 0 \\ \log(|\Delta\mathrm{CFS}| + 1), & \Delta\mathrm{CFS} \geq 0 \end{cases}. \tag{3}$$

Similarly, we also construct functions of $\dot{\tau}'$ and ΔT for better visualization in Figures 4–6c,d:

$$f(\dot{\tau}') = \begin{cases} -\log(|\dot{\tau}'| + 1), & \dot{\tau}' < 0 \\ \log(|\dot{\tau}'| + 1), & \dot{\tau}' \geq 0 \end{cases}, \tag{4}$$

and

$$f(\Delta T) = \begin{cases} -\log(|\Delta T| + 1), & \Delta T < 0 \\ \log(|\Delta T| + 1), & \Delta T \geq 0 \end{cases}. \tag{5}$$

RESULTS

We evaluate the ΔCFS on faults at the depth of 10 km. Tests of evaluation at depth range of 5–15 km yield results with relatively small variations which have no significant effects to our conclusions. We also calculate the cases of $\mu' = 0.0$, 0.4, and 0.8 to illustrate how variation of this parameter would affect the results, and plot the results in Figures 4, 5, and 6.

The calculated CFS changes on faults under the assumption of $\mu' = 0.0$ are shown in Figure 4. The average changes of CFS on the rupture plane of the Lushan earthquake due to coseismic rupture and viscoelastic relaxation of the Wenchuan earthquake are 1.6×10^4 and 1.0×10^3 Pa, respectively. When total stress change is divided by the average tectonic stressing rate of $(2.9 \pm 0.6) \times 10^2$ Pa/year, it appears that the Lushan earthquake was advanced by approximately 59.3 ± 12.3 years by the Wenchuan earthquake. In addition, the coseismic stress change of the Wenchuan earthquake has increased CFS on the Anninghe, Daliangshan, Mabian–Yanjin, and central-southern segments of the Xianshuihe faults by values of 92, 3.3×10^2, 2.1×10^3, and 2.7×10^3 Pa, respectively. During the postseismic deformation process, CFS changes are negative for most of these faults except for the Longmenshan and the central segment of the Xianshuihe faults, on which up to 6.5×10^4 and 2.2×10^3 Pa stress loadings are estimated (Fig. 4b). The total stress changes have significant effects not only at the rupture plane of the Lushan earthquake, but also at the rupture zone of the Wenchuan earthquake and the gap between the two earthquake ruptures, with their earthquake recurring times advanced by approximately 711 ± 203 and 629 ± 126 years, respec-

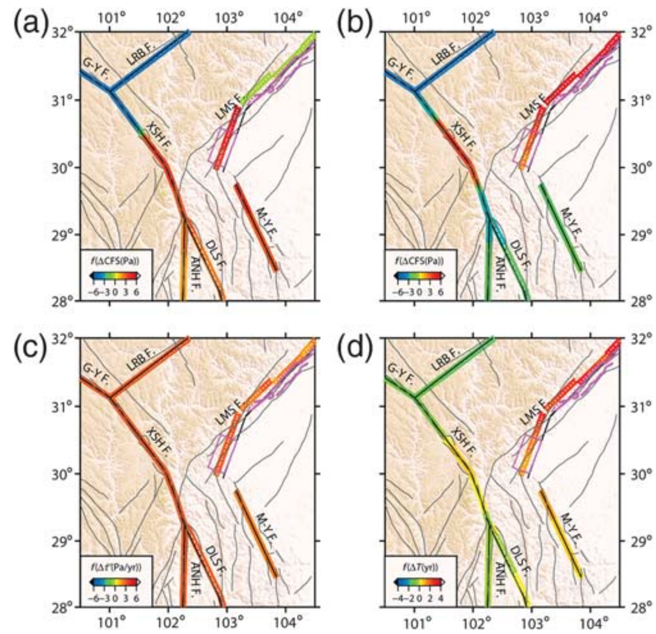

▲ **Figure 4.** ΔCFS caused by the Wenchuan earthquake at 10 km depth assuming $\mu' = 0.0$ and corresponding advance/delay times of earthquake recurrence. (a) and (b) ΔCFS (Pa) induced by coseismic and postseismic loading of the Wenchuan earthquake, respectively. (c) Tectonic stressing rate $\dot{\tau}'$ (Pa/year). (d) Advance/delay times of earthquake recurrence ΔT (years). Gray lines denote active faults. Black solid and white dotted lines show surface traces and the projection of the fault plane at 10 km depth of the modeled faults, respectively. Colors between blue and green stand for decrease of ΔCFS or delay of earthquake recurring times, and between yellow and red for increase of ΔCFS or advance of earthquake recurring times, respectively. The color legends are in logarithmic scale of the absolute ΔCFS. Negative scale stands for decrease of ΔCFS or delay of earthquake recurring times, and positive scale for increase of ΔCFS or advance of earthquake recurring times, respectively.

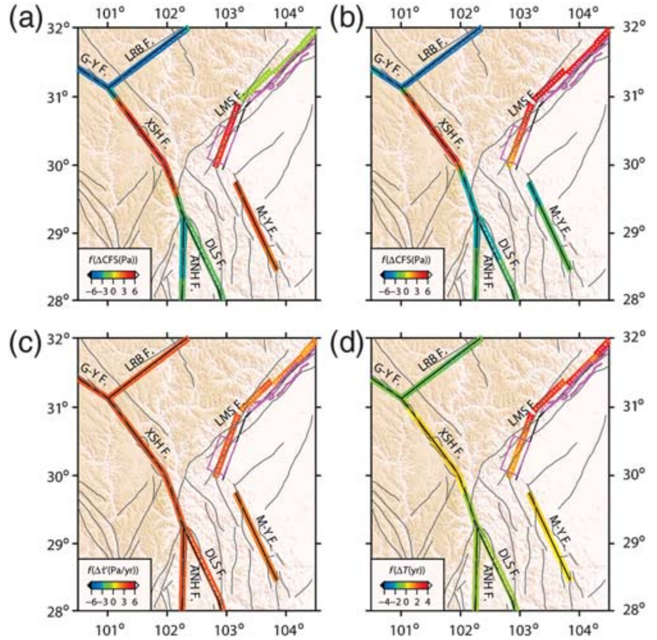

▲ **Figure 5.** ΔCFS caused by the Wenchuan earthquake at 10 km depth assuming $\mu' = 0.4$ and advance/delay times of earthquake recurrence. Legends are the same as that of Figure 4.

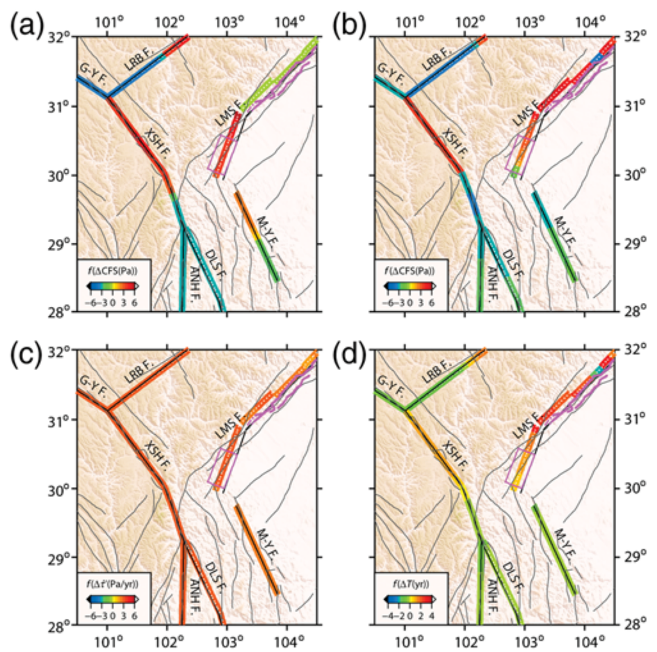

▲ **Figure 6.** ΔCFS caused by the Wenchuan earthquake at 10 km depth assuming $\mu' = 0.8$ and advance/delay times of earthquake recurrence. Legends are the same as that of Figure 4.

tively. Part of the stress loading on the Wenchuan rupture plane is believed to have been released through afterslip, so the total loading effect should be much less than the number indicated. Meanwhile, the advance times of earthquake recurrence on the Mabian–Yanjin and central–southern segment of the Xianshuihe faults due to total stress loading are 5.5 ± 3.2 and 2.1 ± 0.2 years, respectively.

If $\mu' \neq 0$, the normal stresses on faults will contribute to the ΔCFS. The active faults with increased normal stresses induced by the Wenchuan rupture (i.e., corresponding to increases of ΔCFS) are the Longriba and most part of the Xianshuihe faults, with ΔCFSs of 1.5×10^4 and 6.0×10^3 Pa, respectively (Fig. 7a). The CFSs of the two faults are also increased during the five years after the Wenchuan earthquake by 3.3×10^3 and 2.1×10^3 Pa, respectively (Fig. 7b), at fault segments slightly different from the ones with increasing ΔCFSs due to coseismic rupture.

The calculated CFS changes under the assumption of $\mu' = 0.4$ are shown in Figure 5. The average ΔCFSs on the rupture plane of the Lushan earthquake are calculated to be 1.1×10^4 and 6.6×10^2 Pa caused by coseismic and postseismic loading of the Wenchuan earthquake, respectively. When the total stress change is divided by the average tectonic stressing rate of $(2.6 \pm 0.5) \times 10^2$ Pa/year, it appears that the Lushan earthquake was advanced by approximately 45.9 ± 8.8 years by the Wenchuan earthquake. ΔCFSs due to coseismic rupture on the Mabian–Yanjin and most part of the Xianshuihe faults are positive, with values of 1.1×10^3 and 4.3×10^3 Pa, respectively. Positive ΔCFSs are imposed by viscoelastic relaxation on most part of the Xianshuihe (3.0×10^3 Pa) and Longmenshan faults (7.8×10^4 and 8.7×10^3 Pa for the Wenchuan earthquake rupture zone and the gap zone between the two earthquake ruptures), respectively. The total stress changes have similar effects to that under the assumption of $\mu' = 0.0$, with advance times of earthquake recurrence of 577 ± 165 and 534 ± 107 years at the rupture zone of the Wenchuan earthquake and the gap zone between the two events. In addition, the recurring times of the Mabian–Yanjin and the central–southern segment of the Xianshuihe faults are advanced slightly.

We test another case assuming apparent friction coefficient $\mu' = 0.8$, and evaluate the ΔCFSs on fault planes at 10 km depth. Figure 6 shows the ΔCFS result. The corresponding advance time of earthquake recurrence due to the Wenchuan earthquake at the rupture zone of the Lushan earthquake is estimated to be 28.4 ± 5.7 years. Comparing the ΔCFS estimates assuming $\mu' = 0.8$ with that of $\mu' = 0.4$ (Fig. 5 versus 6), we find that most of the ΔCFS estimates do not change much, or at least the senses of ΔCFS are not changed. Causes of the changes are the differential normal stresses between the two cases that are identical to the differences between the two cases of $\mu' = 0.0$ and 0.4, as shown in Figure 7.

We assess triggering effect of the Wenchuan earthquake to the Lushan earthquake based on the ΔCFS and stress loading rate results given above. Because of stress loading caused by the Wenchuan earthquake, the Lushan earthquake may have been advanced for approximately 28.4–59.3 years depending on the assumption of equivalent friction coefficient of the fault plane. This means that the stress loading due to the Wenchuan earthquake is about 5.8–12.1 times of the tectonic loading during the time interval between the two events. We propose a measure for investigating to what extent one earthquake could be

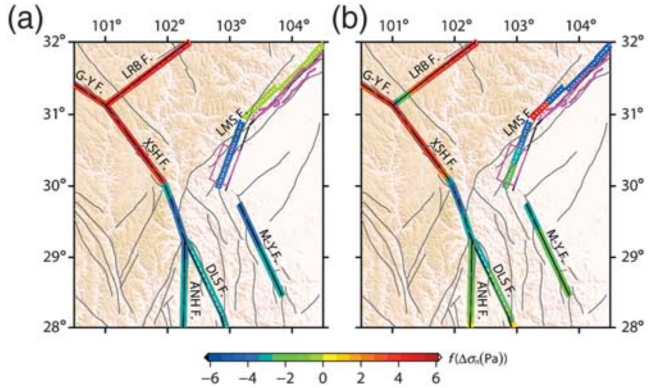

▲ **Figure 7.** (a) and (b) Normal stress $\Delta\sigma_n$ (Pa) induced by coseismic and postseismic loading of the Wenchuan earthquake, respectively. Legends are the same as that of Figure 4.

considered as an aftershock of a previous event, that is, the percentage of stress loading induced by the previous event in total stress loading (tectonic + earthquake induced). In this sense, the Lushan earthquake should be considered as at least 85% of an aftershock of the Wenchuan earthquake. Most of the time advance is due to the coseismic Coulomb stress increase on fault, but the postseismic Coulomb stress increase also had moderate contribution, equivalent to 1.5–3.4 years of time advance. That is, the viscoelastic loading due to the Wenchuan earthquake during the five years after the event, slowly but progressively increased the Coulomb stress on fault, and brought that to a delayed but ultimate failure.

DISCUSSIONS AND CONCLUSIONS

Comparing with previous studies, our paper uses a revised source model for Coulomb stress change calculation, with improved fault geometry and slip distribution of the Wenchuan earthquake, and a layered rheological structure of the lithosphere. In the latter, elastic and viscous properties are constrained using seismic profile data and GPS postseismic observations (Shen, Wang, *et al.*, 2011). The secular fault slip rates are also reevaluated using an updated GPS velocity dataset. Estimates of the ΔCFS and tectonic loading rates are therefore better estimated than previous studies (e.g., Nalbant and McClosky, 2011). Such results are used to estimate changes of earthquake recurring times, enabling us to assess changes of seismic-hazard potentials due to the Wenchuan earthquake along adjacent faults.

Our assessment of earthquake timing is based on the assumption that earthquake occurrence is determined by the mean Coulomb stress accumulated on a fault plane, which can be decomposed into a secular tectonic loading component and a transient loading component with the latter resulted from coseismic and postseismic stress perturbations. This assumption does not consider some nonlinear effects on earthquake occurrence, such as accelerating failure governed by the rate- and state-dependent friction law of Dieterich (1994) and those modeled by Rydelek and Sacks (1999), which took into account the heterogeneous distribution of fault strength and/or Coulomb stress. Such nonlinear stress loading and earthquake process, however, is difficult to model, because our knowledge is quite limited about the associated factors, such as the distributions of asperities and their friction properties on a fault, and the history of earthquake ruptures and their slip distributions. Ignoring such nonlinear processes of earthquake occurrence makes our modeling result and its associated estimate of earthquake triggering less definitive. Nevertheless, our result should be meaningful statistically, as our model based on the linear deformation and loading assumption should provide a first-order assessment of the problem. For assessing whether the Lushan earthquake is an aftershock of the Wenchuan earthquake, we focus on the comparison between triggering effect of the transient stress loading induced by the Wenchuan earthquake and that of tectonic stress loading, and thus provide a quantitative assessment for the aftershock component of the Lushan earthquake. Our conclusion on this is related to our assumption on earthquake occurrence, but is less sensitive to that assumption than those studies focusing on earthquake potentials.

In conclusion, we evaluate the Coulomb stress change at the rupture zone before the Lushan earthquake due to coseismic rupture and postseismic stress relaxation of the 2008 Wenchuan earthquake, and compare that with the tectonic loading Coulomb stress on the fault accumulated since the Wenchuan earthquake. Our results indicate that the Wenchuan induced coseismic and postseismic stress loading significantly increased the earthquake potential before the Lushan earthquake compared to the long-term tectonic loading, resulting in an advance on its occurrence of 28.4–59.3 years depending on the friction coefficient assumption. We conclude that the Lushan earthquake is at least 85% of a delayed aftershock of the Wenchuan earthquake. Our result is qualitatively consistent with that of Jia *et al.* (2014), who estimated about 62% possibility of the Lushan earthquake being an aftershock of the Wenchuan earthquake. They reached the conclusion through statistical analysis of regional seismicity change due to direct and indirect triggering of the Wenchuan earthquake. They also calculated the Coulomb stress change due to coseismic and postseismic stress loading of the Wenchuan earthquake, and obtained results qualitatively consistent with ours. The differences in the actual values of Coulomb stress changes are perhaps due to employment of somewhat different earthquake rupture distribution and media property models in the calculation.

In this paper, we also examine the distribution of Wenchuan induced Coulomb stress change on the neighborhood faults for assessment of earthquake potential of the region. The result shows that earthquake potentials on the Xianshuihe and Mabian–Yanjin faults are slightly increased, whereas the stress levels on the Ganzi–Yushu, Longriba, Anninghe, and Daliangshan faults are decreased. Significant Coulomb stress increase is found in the seismic gap between the Wenchuan and Lushan fault ruptures, which is equivalent to 407–629 years of advancement of earthquake recurrence. Special attention is needed for its midterm earthquake potential.

DATA AND RESOURCES

The GPS data used in this paper are from the Crustal Motion Observation Network of China project and its successor the Continental Tectonic Environmental Monitoring Network of China project, and from the National Basic Research project. These data were observed during 1999–2011. We processed these data to derive a horizontal-velocity field, which is Ⓔ provided in the supplementary material (Table S1). The rupture zone of the 2013 Lushan earthquake adopted in our model is resolved using coseismic displacements observed by GPS by Z. Jiang, M. Wang, Y. Wang, Y. Wu, S. Che, Z.-K. Shen, R. Burgmann, J. Sun, Y. Yang, H. Liao, and Q. Li.

ACKNOWLEDGMENTS

We thank Zhigang Peng and Huajian Yao for their editing work on this special issue of *Seismological Research Letters*. We also appreciate an anonymous reviewer for providing comments that greatly improved the manuscript. We are grateful to Rongjiang Wang for providing and helping us to use the PSGRN/PSCMP code. This paper was supported by grants from the Natural Science Foundation of China (41104008), the China Earthquake Administration (IGCEA1011), and the Natural Science Foundation of China (41090294). Figures in this paper utilized the Generic Mapping Tools (GMT) mapping software of Wessel and Smith (1991).

REFERENCES

Chéry, J., S. Carretier, and J. F. Ritz (2001). Postseismic stress transfer explains time clustering of large earthquakes in Mongolia, *Earth Planet. Sci. Lett.* **94,** 277–286.

Deng, Q. D., Y. Ran, X. Yang, W. Min, and Q. Chu (2007). *Active Tectonics Map of China*, Seismological Press, Beijing.

Dieterich, J. (1994). A constitutive law for rate of earthquake production and its application to earthquake clustering, *J. Geophys. Res.* **99,** no. B2, 2601–2618.

Du, F., F. Long, X. Ruan, G. Yi, Y. Gong, M. Zhao, Z. Zhang, H. Qiao, Z. Wang, and J. Wu (2013). The M 7.0 Lushan earthquake and the relationship with the M 8.0 Wenchuan earthquake in Sichuan, China, *Chin. J. Geophys.* **56,** no. 5, 1772–1783, doi: 10.6038/cjg20130535.

Freed, A. M. (2005). Earthquake triggering by static, dynamic, and postseismic stress transfer, *Ann. Rev. Earth Planet. Sci.* **33,** 335–367, doi: 10.1146/annurev.earth.33.092203.122505.

Freed, A. M., and J. Lin (2001). Delayed triggering of the 1999 Hector Mine earthquake by viscoelastic stress transfer, *Nature* **411,** 180–183.

Gomberg, J., and K. Felzer (2008). A model of earthquake triggering probabilities and application to dynamic deformations constrained by ground motion observations, *J. Geophys. Res.* **113,** B10317, doi: 10.1029/2007JB005184.

Han, L., X. Zeng, C. Jiang, S. Ni, H. Zhang, and F. Long (2014). Focal mechanisms of the 2013 M_w 6.6 Lushan, China earthquake and high-resolution aftershock relocations, *Seismol. Res. Lett.* **85,** no. 1, doi: 10.1785/0220130083.

Harris, R. A. (1998). Introduction to special section, stress triggers, stress shadows, and implications for seismic hazard, *J. Geophys. Res.* **103,** 24,347–24,358.

Jia, K., S. Zhou, J. Zhuang, and C. Jiang (2014). Possibility of the independence between the 2013 Lushan earthquake and the 2008 Wenchuan earthquake on Longmen Shan fault, Sichuan, China, *Seismol. Res. Lett.* **85,** no. 1, doi: 10.1785/0220130115.

King, G. C. P., R. S. Stein, and J. Lin (1994). Static stress changes and the triggering of earthquakes, *Bull. Seismol. Soc. Am.* **84,** 935–953.

Liu, J., G. Yi, Z. Zhang, Z. Guan, X. Ruan, F. Long, and F. Du (2013). Introduction to the Lushan, Sichuan M 7.0 earthquake on 20 April 2013, *Chin. J. Geophys.* **56,** no. 4, 1404–1407, doi: 10.6038/cjg20130434.

Luo, G., and M. Liu (2010). Stress evolution and fault interactions in eastern Tibet: Implications for the 2008 M_w 7.9 Wenchuan earthquake, *Tectonophysics* doi: 10.1016/j.tecto.2009.12.019.

Nalbant, S. S., and J. McCloskey (2011). Stress evolution before and after the 2008 Wenchuan, China earthquake, *Earth Planet. Sci. Lett.* **307,** 222–232.

Okada, Y. (1992). Internal deformation due to shear and tensile faults in a half-space, *Bull. Seismol. Soc. Am.* **82,** 1018–1040.

Parsons, P., C. Ji, and E. Kirby (2008). Stress changes from the 2008 Wenchuan earthquake and increased hazard in the Sichuan basin, *Nature* **454,** 509–510, doi: 10.1038/nature07177.

Parsons, T., and M. Segou (2014). Stress, distance, magnitude, and clustering influences on the success or failure of an aftershock forecast: The 2013 M 6.6 Lushan earthquake and other examples, *Seismol. Res. Lett.* **85,** no. 1, doi: 10.1785/0220130100.

Pollitz, F., and I. S. Sacks (2002). Stress triggering of the 1999 Hector mine earthquake by Transient deformation following the 1992 Landers earthquake, *Bull. Seismol. Soc. Am.* **92,** no. 4, 1487–1496.

Rice, J. R. (1992). Fault stress states, pore pressure distribution, and the weakness of the San Andreas fault, in *Fault Mechanics and Transport Properties of Rock*, B. Evans and T. F. Wong (Editors), Academic Press, London, 475–503.

Rydelek, P. A., and I. S. Sacks (1999). Large earthquake occurrence affected by small stress changes, *Bull. Seismol. Soc. Am.* **89,** no. 3, 822–828.

Savage, J. C., and R. O. Burford (1973). Geodetic determination of relative plate motion in central California, *J. Geophys. Res.* **78,** no. 5, 832–845, doi: 10.1029/JB078i005p00832.

Shen, Z.-K., R. W. King, D. C. Agnew, M. Wang, T. A. Herring, D. Dong, and P. Fang (2011). A unified analysis of crustal motion in Southern California, 1970–2004: The SCEC crustal motion map, *J. Geophys. Res.* **116,** no. B11, doi: 10.1029/2011JB008549.

Shen, Z. K., J. Sun, P. Zhang, Y. Wan, M. Wang, R. Bürgmann, Y. Zeng, W. Gan, H. Liao, and Q. Wang (2009). Slip maxima at fault junctions and rupturing of barriers during the 2008 Wenchuan earthquake, *Nature Geosci.* **2,** 718–724, doi: 10.1038/NGEO636.

Shen, Z., F. Wang, M. Wang, Y. Wan, P. Zhang, J. Sun, W. Tao, Y. Wang, K. Wang, and M. Hao (2011). Postseismic deformation of the 2008 M_w 7.9 Wenchuan earthquake and its tectonic implications, *AGU Fall Meeting*, San Francisco, California, 5–9 December 2011, Abstract T31E-07.

Steacy, S., J. Gomberg, and M. Cocco (2005). Introduction to special section: Stress transfer, earthquake triggering, and time-dependent seismic hazard, *J. Geophys. Res.* **110,** B05S01, doi: 10.1029/2005JB003692.

Stein, R. S. (1999). The role of stress transfer in earthquake occurrence, *Nature* **402,** 605–609.

Stein, R. S., G. C. P. King, and J. Lin (1992). Change in failure stress on the southern San Andreas fault system caused by the 1992 magnitude 7.4 Landers earthquake, *Science* **258,** 1328–1332.

Toda, S., J. Lin, M. Meghraoui, and R. S. Stein (2008). 12 May 2008 M 7.9 Wenchuan, China, earthquake calculated to increase failure stress and seismicity rate on three major fault systems, *Geophys. Res. Lett.* **35,** L17305, doi: 10.1029/2008GL034903.

Wan, Y., and Z. K. Shen (2010). Static Coulomb stress changes on faults caused by the 2008 M_w 7.9 Wenchuan, China earthquake, *Tectonophysics* **491,** 105–118.

Wang, Q., X. Qiao, Q. Lan, F. Jeffrey, S. Yang, C. Xu, Y. Yang, X. You, K. Tan, and G. Chen (2011). Rupture of deep faults in the 2008 Wenchuan earthquake and uplift of the Longmen Shan, *Nat. Geosci.* **4,** 634–640, doi: 10.1038/ngeo1210.

Wang, R., F. Lorenzo-Martín, and F. Roth Frank (2006). PSGRN/PSCMP—A new code for calculating co- and post-seismic deformation, geoid and gravity changes based on the viscoelastic-gravitational dislocation theory, *Comput. Geosci.* **32,** 527–541.

Wang, W., J. Hao, and Z. Yao (2013). Preliminary result for rupture process of April 20, 2013, Lushan earthquake, Sichuan, China, *Chin. J. Geophys.* **56,** no. 4, 1412–1417, doi: 10.6038/cjg20130436.

Wessel, P., and W. H. F. Smith (1991). Free software helps map and display data, *Eos Trans. AGU* **72,** no. 41, 441–446.

Xu, C. J., J. Wang, Z. Li, and J. Dummond (2010). Applying the Coulomb failure function with an optimally oriented plane to the 2008 M_w 7.9 Wenchuan earthquake triggering, *Tectonophysics* **491,** 119–126.

Xu, X., G. Chen, G. Yu, J. Cheng, X. Tan, A. Zhu, and X. Wen (2013). Seismogenic structure of Lushan earthquake and its relationship with Wenchuan earthquake, *Earth Science Frontiers (Di Xue Qian Yuan)* **20,** no. 3, 11–20.

Zhang, Y., R. Wang, Y.-T. Chen, L. Xu, F. Du, M. Jin, H. Tu, and T. Dahm (2014). Kinematic rupture model and hypocenter relocation of the 2013 M_w 6.6 Lushan earthquake constrained by strong-motion and teleseismic data, *Seismol. Res. Lett.* **85,** no. 1, doi: 10.1785/0220130126.

Yanzhao Wang
Min Wang
State Key Laboratory of Earthquake Dynamics
Institute of Geology
China Earthquake Administration
Beijing 100029, China
wangyz0513@gmail.com
mwang@gps.gov.cn

Fan Wang
National Geomatics Center of China
Beijing 100830, China
wangfan0003@gmail.com

Zheng-Kang Shen[1]
Department of Earth and Space Sciences
University of California, Los Angeles
Los Angeles, California 90095-1567 U.S.A.
zshen@ucla.edu
zhengkangshen@pku.edu.cn

Yongge Wan
Institute of Disaster Prevention Science and Technology
Yanjiao, Sanhe City
Hebei Province 065201, China
wanyg217217@vip.sina.com

[1] Also at School of Earth and Space Science, Peking University, Beijing 100871, China.